AIP | Review of Scientific Instruments

Use of one dimensional Dα camera to measure edge electron density gradients

M. R. Tournianski, P. G. Carolan, N. J. Conway, G. F. Counsell, E. Arends et al.

Citation: Rev. Sci. Instrum. **74**, 2089 (2003); doi: 10.1063/1.1537041

View online: http://dx.doi.org/10.1063/1.1537041

View Table of Contents: http://rsi.aip.org/resource/1/RSINAK/v74/i3

Published by the American Institute of Physics.

Use of one dimensional D_α camera to measure edge electron density gradients

M. R. Tournianski,[a] P. G. Carolan, N. J. Conway, and G. F. Counsell
EURATOM-UKAEA Fusion Association, Culham Science Centre, Abingdon, Oxfordshire OX14 3DB, United Kingdom

E. Arends
FOM Institute for Plasma Physics "Rijnhuizen," P.O. Box 1207, 3430 BE Nieuwegein, Netherlands

M. J. Walsh
Walsh Scientific Ltd., Culham Science Centre, Abingdon, Oxfordshire OX14 3EB, United Kingdom

(Presented on 10 July 2002)

One of the clearest signatures of the transitions from *L*- to *H*-mode plasmas is the steepening of the edge density gradient. A concomitant narrowing of the visible radiation, usually dominated by Balmer D_α emission, is generally observed. Typically, the D_α emissivity width is 4–6 cm for the *L*-mode, similar for ELMs, and 1–3 cm for *H*-mode MAST plasmas, comparable with typical edge n_e scale lengths. A means of extracting electron densities from this narrowing of the radial D_α emissivity profile was pioneered on the START device and developed further on MAST. It takes advantage of the near insensitivity to electron temperature of both the ionization and emission rates of hydrogen at temperatures well in excess of the ionization potential (13.6 eV). The D_α emissivity profile is obtained from spatial inversion of line-of-sight integrated intensities recorded by a linear camera ($\Delta t = 125\ \mu$s, 256 pixels). The 300 point Thomson scattering diagnostic has been used as a yardstick in comparing experimental data from a wide range of edge density gradients and a range of edge temperatures in checking the models validity and assumptions. [DOI: 10.1063/1.1537041]

I. INTRODUCTION

Over the past few years fusion research has enjoyed exciting advances in tokamak plasma physics. This progress places extra demands for accurate measurements of the radial profiles at the plasma edge. Edge electron density is a key factor in understanding many edge dominated phenomena such as *H*-mode access and dynamics, fueling efficiency, and neutral particle beam injection (NBI) edge losses. Because of the crucial importance of such measurements, a state-of-the-art Thomson scattering (TS) diagnostic system[1] has been implemented on the MAST tokamak. This provides a single time point measurement of electron temperature and density in 300 radial locations delivering high spatial resolution at the plasma edge. However, in MAST, like other medium tokamaks, high power lasers with limited pulse repetition rate are required in order to provide sufficient photon statistics in wide range of electron densities. Also, the increasing physics demands in tokamaks emphasis the importance of almost uninterrupted monitoring of the edge density profile. One approach is to employ high repetition rate lasers with multipoint scattering access, which we are pursuing in MAST,[1] but here we take a complementary approach. The advantages of the simple atomic physics of hydrogen ionization and excitation are exploited to provide a simple, robust, and inexpensive method for extracting the edge electron density gradients. We use the TS measurements to check the validity of assumptions and models used. The method is based on the atomic physics interpretation of the radial D_α emissivity, reconstructed from the linear charge coupled device (CCD) camera data which monitors the plasma edge emission with high time resolution. This diagnostic has already been successfully used on START and MAST to measure the position of the plasma edge and obtain the neutral density profile when the n_e and T_e profiles are available by Thomson scattering.

The application of the proposed technique is naturally limited by the position of the D_α emission source function, which normally is a few centimeters wide and located close to the edge of the plasma. Some simplification for the edge n_e profile is required in order to construct a simple and robust model for the radial D_α emissivity. Nevertheless, the radial width of the D_α emissivity full width at half maximum (FWHM) is comparable with typical edge n_e scale lengths in both START and MAST and can be extracted with very high time resolution, in real time if necessary, providing information about the plasma edge density behavior throughout the discharge.

II. INSTRUMENTATION AND INVERSION TECHNIQUE

The pioneering START device, and its scaled-up version MAST with plasma cross section comparable to ASDEX-U and DIII–D, have a wide operational density space, with typical central densities between 10^{19} and $10^{20}\ m^{-3}$, are a testing ground for the proposed technique. Both tokamaks have a distinctive design feature, where the outboard plasma

[a]Electronic mail: mikhail.tournianski@ukaea.org.uk

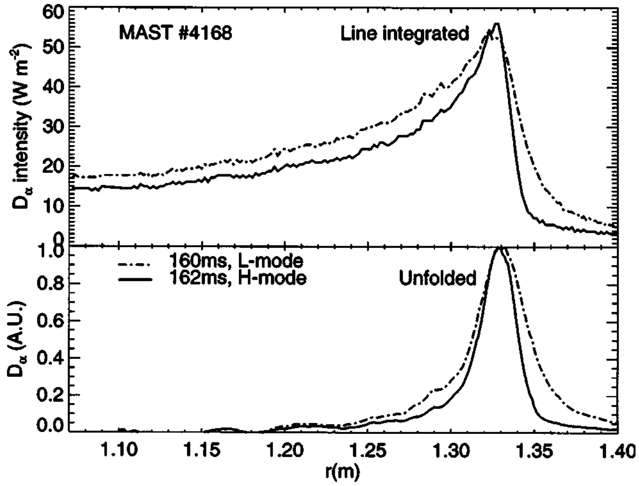

FIG. 1. Line-integrated D_α intensity (top) ($\Delta t = 1$ ms) and radially unfolded D_α emissivity profiles (bottom) during L and H phases of a MAST plasma.

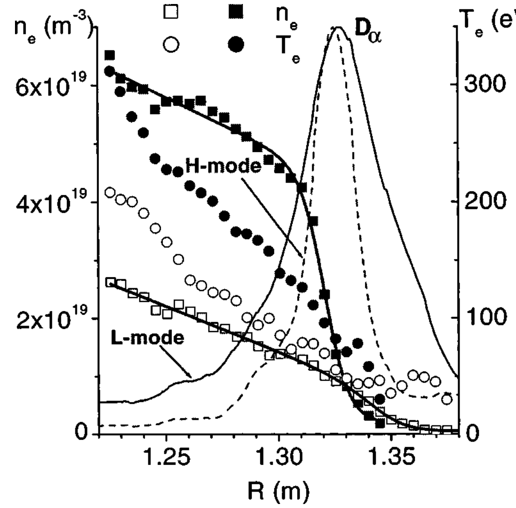

FIG. 2. Normalized radially unfolded D_α emissivity profiles for two MAST discharges with contrasting edge n_e gradients. The T_e profiles are also presented and show less change.

edge and tokamak vessel are separated by a significant distance, providing access for multichord optical diagnostic viewing beyond the plasma edge.

To record the radial D_α emissivity an absolutely calibrated D_α linear CCD camera (256 elements) has been installed. The camera images the entire midplane of the START machine and the outboard plasma range on MAST ($1.07\ \text{m} < R < 1.53\ \text{m}$) with ~ 10 and ~ 2 mm spatial resolution, respectively. The time resolution, Δt, is mainly limited by the CCD readout speed and allows $\Delta t \geq 125\ \mu\text{s}$. The camera views the plasma in the equatorial plane and is spectrally filtered for emission within the D_α wavelength range by placing an interference filter in front of the lens of the CCD array. In order to suppress wall reflections, the walls of both START and MAST were blackened using colloidal graphite.

Typical profiles of the line-of-sight integrated intensities obtained from the D_α linear camera are shown in Fig. 1 for L- and H-mode plasmas in MAST (No. 4168, $t = 160$ ms and $t = 162$ ms). Inverting the line-of-sight integrated intensities allows the local D_α emissivity distribution to be determined, in principle. Assuming toroidal symmetry and calculating the contributions from radial annuli to each of the viewing chords produces a set of linear equations. The algorithm automatically incorporates the radial smearing from the optics including the finite CCD element size. A number of matrix inversion algorithms are used to produce the solution matrix. We generally use "singular value decomposition" to avoid numerical roundoff problems but a simple Abel inversion gives almost identical results due to the narrow pencil beam optics for each camera pixel detector.

The corresponding inverted D_α emissivity profiles are shown at the bottom of Fig. 1, and seen to narrow to ~ 2 cm FWHM in 2 ms during the L to H transition, consistent with an increased ionization rate from a steepening of the edge electron density gradient. This narrowing is also clearly visible on the raw, prior unfolding, data from the linear CCD camera, shown at the top of Fig. 1, illustrating significant changes in radial profiles of line-of-sight integrated intensities during the MAST L- to H-mode transition.

The T_e and n_e radial distributions are obtained from the 300 point Thomson scattering system with an average spatial resolution of $\Delta r \approx 5$ mm.[1] An estimate of the neutral influx velocity is derived from D_α Doppler spectroscopy measurements of edge neutrals giving an effective $T_0 \sim 1-2$ eV,[2] typical of the edge neutrals for other tokamaks.

III. METHOD

The Balmer-α spectral line is generally the dominant source of visible emission at the tokamak plasma edge. The main feature of a typical Balmer-α spectrum is the cold ($\sim$1–2 eV) emission line from the neutral H and D atoms from the plasma edge at $\lambda_H = 656.28$ nm and $\lambda_D = 656.11$ nm. The strong correlation between the narrowing of the radial D_α emissivity profiles and steepening of the electron pressure are well known and have been observed on many major tokamaks. Two MAST discharges with edge n_e gradients $\sim 2\times 10^{21}$ and 3×10^{20} m^{-4} are compared in Fig. 2 together with multipoint TS[1] measurements of $n_e(r)$, and normalized radial profiles of unfolded D_α emissivity. There is a clear narrowing of the D_α emissivity accompanying the rise in the edge n_e gradient.

The radial D_α emissivity profile (i.e., D_α source function) can be presented as the product of the neutral and electron densities and the effective rate coefficient $\langle \sigma v \rangle_{ex}$ for populating the $n = 3$ principal quantum level

$$D_\alpha = n_e n_0 \langle \sigma v \rangle_{\text{ex}}. \tag{1}$$

The observed changes in D_α emissivity profile are primarily due to the increased electron density gradients at the edge and much less sensitively dependent on changes in the $T_e(r)$ profile. Typically, the T_e ranges between 40 and 200 eV for most of the D_α emissivity in START and MAST plasmas, where ion and impurity impact ionization is negligible, and well in excess of the hydrogen ionization potential (13.6 eV) making the rate coefficients almost temperature independent. Both the effective ionization rate, $\langle \sigma v \rangle_{\text{ion}}$, responsible for n_0 attenuation in the plasma edge and the excitation rate,

$\langle \sigma v \rangle_{ex}$, for populating the $n=3$ principal quantum level, vary by only $\sim$15% in the typical radial scale length of D_α emissivity.[3] For example, at typical edge densities around $\sim 10^{19}\ \mathrm{m}^{-3}$ the effective rate will only rise from $\sim 2.1 \times 10^{-15}$ to $\sim 2.5\times 10^{-15}\ \mathrm{m^3\,s^{-1}}$ for excitation and from $\sim 2.5\times 10^{-14}$ to $\sim 3.1\times 10^{-14}\ \mathrm{m^3\,s^{-1}}$ for electron impact ionization in the temperature range between 40 and 200 eV.

Taking advantage of these atomic physics effects, the edge D_α emissivity profile can be readily estimated from densities alone. For the sake of simplicity and as a preliminary estimate we have developed a simple 1D analytical model illustrating the behavior of the FWHM of the radial D_α emissivity profile, Δ_α, as a function of the plasma edge parameters.

We neglect charge–exchange recombination and assume that neutrals at the plasma edge can be lost only due to collisions with electrons. The neutral density can then be derived from the particle continuity

$$\frac{\partial n_0}{\partial t} + \nabla \boldsymbol{\Gamma}_0 = -S, \tag{2}$$

where $\boldsymbol{\Gamma}_0$ is the neutral flux and S represents neutral losses due to ionization. The diffusive term in particle flux, $\boldsymbol{\Gamma}_0$ is estimated to be substantially smaller than the convective term and can be neglected, i.e., $\boldsymbol{\Gamma}_0 = \mathbf{V}_0 n_0$, where $\mathbf{V}_0$ is the neutral influx velocity. Therefore, the edge neutral density can be derived by solving the differential equation for steady state conditions:

$$\mathbf{V}_0 \cdot \nabla n_0 + n_e n_0 \langle \sigma v \rangle_{\mathrm{ion}} = 0, \tag{3}$$

where V_0 is the neutral influx velocity. The edge n_e density profile is represented by a simple linear approximation, $n_e = dn_e/dr \cdot r$. In a 1D approximation the solution n_0 to Eq. (3) takes a Gaussian form and is given by

$$n_0 = n_0(0)\exp\left(-\frac{\langle \sigma v \rangle_{\mathrm{ion}}}{2V_0} \frac{dn_e}{dr} r^2 \right), \tag{4}$$

where r is the distance from the plasma edge and $n_0(0)$ is the edge neutral density.

In this assumption the radial D_α emissivity profile can be approximated by

$$D_\alpha = \frac{dn_e}{dr} \cdot r \cdot n_0(0) \exp\left(-\frac{\langle \sigma v \rangle_{\mathrm{ion}}}{2V_0} \frac{dn_e}{dr} r^2 \right) \langle \sigma v \rangle_{\mathrm{ex}}. \tag{5}$$

Taking $\langle \sigma v \rangle_{\mathrm{ion}}$ and $\langle \sigma v \rangle_{ex}$ to be constant in the D_α emissivity range, i.e., neglecting the very weak temperature dependence, the position of the maximum of the radial D_α emissivity, r_α, can be found by differentiating Eq. (5):

$$r_\alpha = \sqrt{\frac{V_0}{\langle \sigma v \rangle_{\mathrm{ion}} \cdot dn_e/dr}}. \tag{6}$$

Using Eq. (6) and expressing the D_α emissivity at a position half maximum, r_Δ, Eq. (5) can be rewritten as

$$\xi \exp\left(-\frac{\xi^2}{2} \right) = \frac{1}{2} \exp \frac{1}{2}, \tag{7}$$

where ξ is a dimensionless variable given by

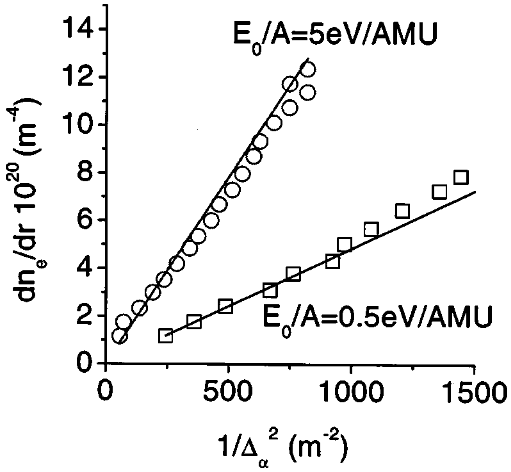

FIG. 3. Computer modeling of $1/\Delta_\alpha^2$ vs dn_e/dr assuming a linear approximation for the edge electron density profile and two different neutral particle influx energies. Solid lines represent the analytic approximation for dn_e/dr.

$$\xi = \sqrt{\frac{\langle \sigma v \rangle_{\mathrm{ion}}}{V_0} \frac{dn_e}{dr}} \cdot r_\Delta. \tag{8}$$

There are two unique solutions of Eq. (7) corresponding to the left- and right-hand side of D_α emissivity at the positions of half maximum. Therefore, the FWHM of D_α emissivity, Δ_α, can be approximated by

$$\Delta_\alpha \approx 1.6 \cdot \sqrt{\frac{V_0}{\langle \sigma v \rangle_{\mathrm{ion}} dn_e/dr}}, \tag{9}$$

thus,

$$\frac{dn_e}{dr} \approx \frac{V_0}{\langle \sigma v \rangle_{\mathrm{ion}}} \left(\frac{1.6}{\Delta_\alpha} \right)^2. \tag{10}$$

This simple analytical approach allows us to relate the edge n_e with the D_α emissivity width, prior to employing more sophisticated atomic and transport modeling. A simple linear relationships between edge n_e gradient gradient, dn_e/dr, and associated emissivity widths $1/\Delta_\alpha^2$ and neutral influx velocity, V_0, has been found [see Eq. (10)], and thus suitable for rapid data analysis and online plasma position control.

The analytical approximations of Δ_α are compared with the computer simulations of the radial D_α emissivity based on the ADAS database.[3] A 1D Monte Carlo neutral particle transport code[2] has been used to model the edge neutral density profile and to test the T_e sensitivity for typical MAST and START plasma edge conditions ($T_e \sim 40$–200 eV). The calculations were performed for two neutral influx energies $E_0/A = 5$ and 0.5 eV/AMU and with random variation of the edge T_e profile. The resulting computer simulations for $1/\Delta_\alpha^2$ are shown in Fig. 3. The modeling results agree with analytical estimates (solid lines in Fig. 3) and show an almost linear dependence of dn_e/dr on $1/\Delta_\alpha^2$ and neutral influx velocity [see Eq. (10)]. The simulated data for the conditions here give $dn_e/dr = b/\Delta_\alpha^2 \cdot \sqrt{E_0/A}$, where $b \sim 6.5 \times 10^{17}\ \mathrm{m^{-2}\,eV^{-1/2}}$, E_0 is the neutral particle influx energy, and A is the atomic mass.

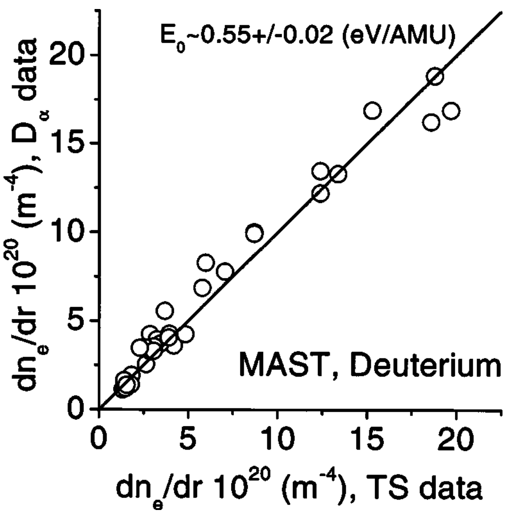

FIG. 4. Experimentally obtained dn_e/dr from D_α emissivity and TS measurements for a number of MAST deuterium discharges.

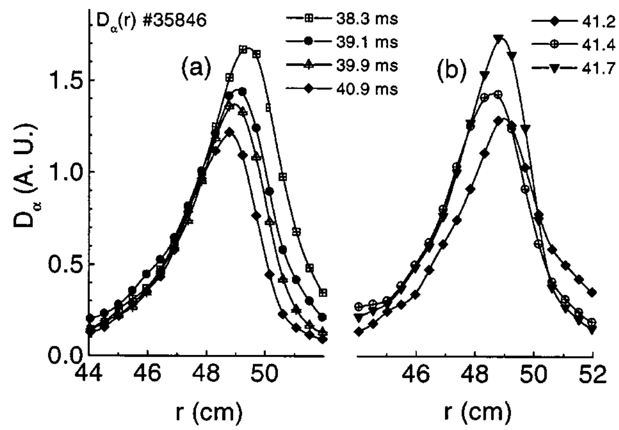

FIG. 5. Evolution of D_α emissivity profiles in START. During the inter-ELM period the full width at half maximum narrows from ~3.5 cm at 38.3 ms (just before the start of inter-ELM period), gradually reaching a minimum of ~2.4 cm at 40.9 ms (a) but broadening again at $t=41$ ms when there was an ELM (b).

A test set of the edge n_e measurements in MAST deuterium discharges has been combined using the 300 point TS diagnostic[1] omitting fast events such as ELMs. For estimating the edge n_e gradients from TS data a modified tanh function[4] least-square fit has been used. Examples of these fits for $n_e(r)$ measurements are plotted as solid lines in Fig. 2. All measurements are taken at the TS time and at the D_α peak position which is normally coincident with the location of the maximum n_e gradient in the tanh fit for a typical MAST discharge. The examined data set of dn_e/dr measurements has a dynamic range of ~15, ranging from $\sim 1.3 \times 10^{20}$ to $\sim 2 \times 10^{21}$ m^{-4}.

Finally, the dn_e/dr from the TS are compared with the results from the linear D_α camera. Good agreement between the two diagnostics has been found and is shown in Fig. 4. The method used and the physics assumptions employed are also strongly supported by the observed linear dependence of dn_e/dr on $1/\Delta_\alpha^2$.

For the data in Fig. 4, the velocity of influx neutrals, V_0, is used as a free parameter in achieving the best linear fit between dn_e/dr from the linear D_α camera and that from the TS, giving an influx energy of $E_0 \sim 0.55$ eV/AMU, in good agreement with experimental observations from Doppler D_α measurements ($T_0 \sim 1$ eV)[2] (this technique can be applied to extract the neutral influx velocity when the edge n_e gradient is known by other means).

In addition to this, the examined data set of dn_e/dr and TS measurements provides an initial estimate of typical errors of the method (see Fig. 4). There are many possible sources for errors in extracting n_e gradients from linear CCD array measurements. The presence of the inversion algorithm introduces additional sources of uncertainties and makes accountability of errors more complicated. First of all there are random errors on spectra, due to both photon and detector noise. Inaccurate calibration of the sensitivities and uncertainties in the collection volumes of the lines of sight can also cause inversion errors. Other emission lines can also be present in the spectra but have a negligible effect due to the relatively high brightness of the Balmer-α transition line. Some of these errors can be characterized by the use of a "Monte Carlo" technique. For example, errors due to noise have been estimated by generating ideal (i.e., noiseless) line integrated intensities using the atomic physics modeling based on the ADAS database and TS data. Then synthetic (i.e., noisy) radial profiles of the line integrated intensities have been generated, using Poisson deviates to model the photon noise and normal deviates for the detector readout noise. The synthetic profiles are then inverted resulting in ~5% errors for extracting Δ_α resulting in an ~10% uncertainty in the n_e gradient. Finally, there are systematic errors associated with a number of physics assumptions, accuracy in effective rate calculations, etc. Most types of systematic errors are difficult to assess. Sensitivity studies have been performed on both real and simulated data in order to evaluate the impact of some of these uncertainties. The results have indicated that the effect of systematic uncertainties is of the same order as the errors due to statistical noise.

IV. EXPERIMENTAL RESULTS

To illustrate the merits of this diagnostic and to demonstrate the applicability of, the described technique for machines of different scale we show results from both START and MAST devices.

The advantages of the fast time response in investigating *H*-mode dynamics were first demonstrated in the START tokamak. The radial D_α emissivity profiles during the inter-ELM period are shown in Fig. 5. The D_α width, Δ_α, gradually reaches a minimum of ~2.4 cm ($t=40.5$ ms), Fig. 5(a), but broadens again starting at $t=41$ ms when there was an ELM [Fig. 5(b)]. The interpretation of the D_α narrowing is presented in Fig. 6 showing a doubling in the n_e gradient from $\sim 6 \times 10^{20}$ to $\sim 1.2 \times 10^{21}$ m^{-4} during the inter-ELM period (~2.75 ms). The line integrated D_α time trace and the poloidal velocity, v_θ, measurements of C^{2+} (464.7 nm) ions obtained at much the same location are also shown for reference.

On MAST, a frequency scanning electron Bernstein wave (EBW) radiometer[5] is used to observe EBW emission.

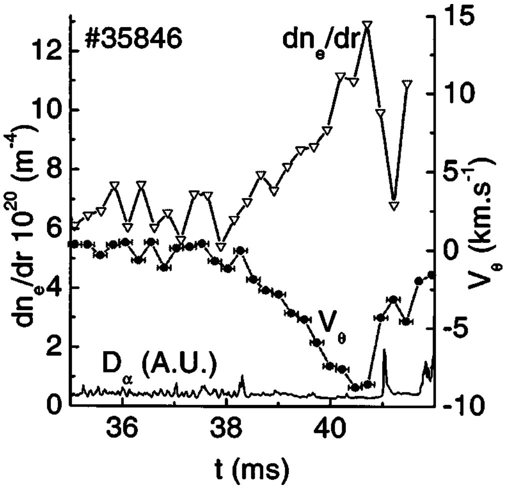

FIG. 6. Comparisons, during H-mode evolution in START, between the poloidal velocity, v_θ from C^{2+}, and the estimated density gradient, dn_e/dr, at the D_α emissivity range position.

Strong overdense plasma emission was observed during *H*-mode operations in MAST, indicating a rise in the edge density gradient. A time history of EBW radiation power observed during inter-ELM periods together with changes in dn_e/dr and the line integrated D_α trace is shown in Fig. 7. A strong correlation between the EBW emission and dn_e/dr is observed (Pearson correlation coefficient ~0.76) showing a buildup of the density gradient during the *H*-mode phase of the discharge with a subsequent decrease in dn_e/dr when the plasma returns to *L* mode. The time enhanced inset in Fig. 7 shows an example of an increase in dn_e/dr during inter-ELM periods with a subsequent reduction in dn_e/dr from $\sim 1.5\times10^{21}$ to $\sim 5\times10^{20}$ m^{-4} when there is an ELM.

The versatility of the proposed diagnostic technique extends beyond extracting dn_e/dr. For example, the energy of influx neutrals may be obtained with high accuracy (see Fig. 4), given the knowledge of the edge electron density. This can be an important factor in improving understanding of gas feed sources of neutrals and other aspects of *H*-mode dynamics. Also, we plan to exploit a simple relationship between the D_α emissivity position and the location of the plasma boundary to control the plasma position and shape using real time analysis in the feedback system in MAST. This innovative approach may be extremely beneficial to resolve some problems associated with pickup coils being remote from the plasma edge. The use of spectroscopic/optical information for position of the plasma boundary may also help to avoid the long integration time from the edge pickup coils in quasicontinuous plasmas, such as ITER.

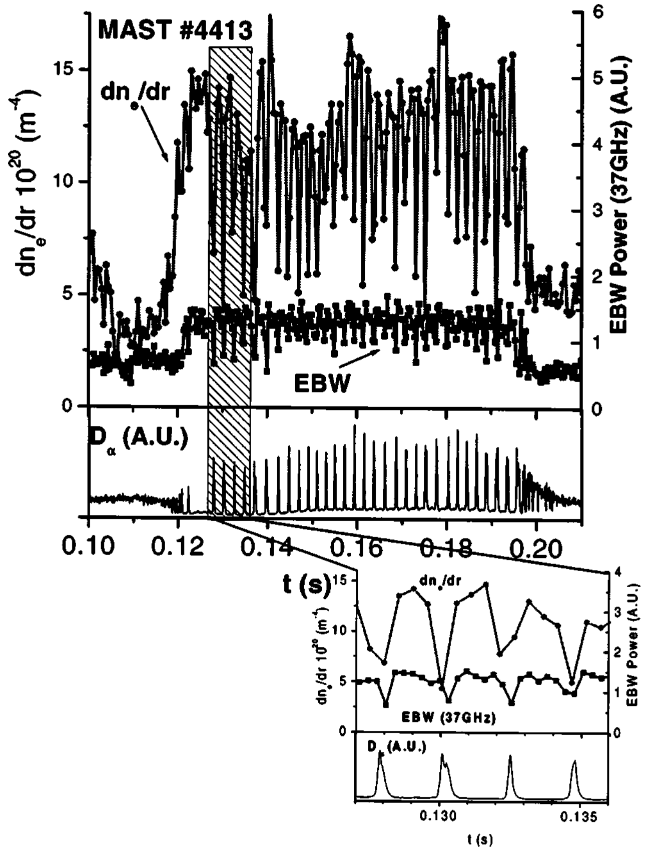

FIG. 7. Evolution of electron Bernstein wave (EBW) radiation power, dn_e/dr and D_α waveforms observed in an ELMy MAST plasma. The time enhanced inset shows an increase in dn_e/dr during inter-ELM periods with a subsequent reduction in dn_e/dr when there is an ELM.

ACKNOWLEDGMENTS

The authors would like to thank J. Dowling, H. Meyer, and V. Shevchenko for their technical contributions. This work is funded by the U.K. Department of Trade and Industry and EURATOM.

[1] M. J. Walsh *et al.*, Rev. Sci. Instrum. (these proceedings).
[2] M. R. Tournianski, P. G. Carolan, N. J. Conway, G. F. Counsell, A. R. Field, and M. J. Walsh, Nucl. Fusion **41**, 77 (2001).
[3] H. P. Summers, Atomic Data and Analysis Structure, JET Report, JET-IR(94) 06, 1994.
[4] R. J. Groebner and T. N. Carlstron, Plasma Phys. Controlled Fusion **40**, 673 (1998).
[5] V. Shevchenko, G. Cunningham, and A. Field, Proceedings of 28th EPS Conference, 2001, Vol. 25A, p. 1285.